INSTITUTE OF PHYSICS PUBLISHING JOURNAL OF PHYSICS B: ATOMIC, MOLECULAR AND OPTICAL PHYSICS

J. Phys. B: At. Mol. Opt. Phys. **39** (2006) 3665–3678 doi:10.1088/0953-4075/39/17/022

Low-energy single electron capture, target excitation and ionization in He^{2+} + Na(3s) collisions

Teck-Ghee Lee

Physics Division, Oak Ridge National Laboratory, Oak Ridge, TN 37831, USA
and
Department of Physics and Astronomy, University of Kentucky, Lexington, KY 40506, USA

E-mail: leetg@ornl.gov

Received 12 June 2006
Published 29 August 2006
Online at stacks.iop.org/JPhysB/39/3665

Abstract

Extensive semiclassical atomic orbitals close-coupling calculations have been performed to investigate single electron capture, excitation and ionization cross sections for He^{2+} + Na(3s) collisions from 2 to 20 keV u^{-1}. Special attention was paid to transition channels where significant discrepancies among theories and experiments were reported in this energy region. The stability of the calculated inelastic cross sections with respect to the choice of basis functions has been examined. The present calculations for single electron capture, target excitation and ionization cross sections are found to be in good agreement with existing experimental data, as well as with previous theoretical calculations. In particular, the total ionization and partial electron capture cross sections into $n = 2, 3, 4$ and $n \geqslant 5$ shells are in excellent agreement with the recent experimental measurements performed using the MOTRIMS technique (Knoop *et al* 2005 *J. Phys. B: At. Mol. Opt. Phys.* **38** 1987).

(Some figures in this article are in colour only in the electronic version)

1. Introduction

Studies of electron capture, target excitation and ionization processes in collisions between alkali-metal atoms (e.g., Li, Na, K, Rb, . . .) and singly or multiply charged ions in the ground state as well as in excited states are attractive for two reasons. First, from the fundamental point of view, like H atoms, alkali-metal atoms are essentially quasi one-electron atoms since their outermost electron is loosely bound with respect to the rest of their inner-shell electrons. Second, from the experimental point of view, it is relatively easier to handle alkali-metal atoms compared to H atoms. Furthermore, such collision systems can serve as a fundamental testing ground for many theoretical models.

Numerous experiments [1–4] have been carried out to determine electron transfer, target excitation and ionization cross sections for the $H^+ + Na$ system. In the low-energy region, due to the difficulties in manipulating ion beams, most experimental measurements were performed at energy above 10 keV u^{-1}. Experimental results for energies ranging between 10 and 500 keV u^{-1} are relatively well described by various elaborate theoretical methods that have been developed over recent decades. Between 1 and 10 keV u^{-1}, however, a complete theoretical description of electron capture, excitation and ionization in singly or multiply charged ion and atom collision systems remains a challenge even with modern advanced computing power.

Generally, a basis set expansion coupled-channel method, equipped with a sufficiently large number of basis functions, is able to accurately determine the cross sections for the dominant transition channels. For the less dominant channels such as ionization, which is a weak process below 10 keV u^{-1}, and having a cross section that is small compared to the resonant electron capture or even excitation processes, employing of a large basis set still may be necessary to obtain reasonable inelastic cross sections in the low-energy region. The impediments associated with utilizing such a huge number of basis functions in the close-coupling method are (i) the long hours of computation time; (ii) the stability of the two-centre matrix elements evaluation and (iii) numerical convergence associated with the size of the basis sets. However, these impediments have never stopped attempts to compute reasonable inelastic cross sections. For example, Jain and Winter [5] have done a thorough study of the electron capture, excitation and ionization cross sections for $H^+ + Na(3s \text{ and } 3p)$ between 1 and 100 keV u^{-1} impact energy using the two-centre coupled Sturmian-pseudostates atomic-orbital close-coupling (SAOCC) method. Their results were in good agreement with the existing measurements and other theoretical calculations for most of the inelastic transitions. Being successful in using the two-centre coupled Sturmian-pseudostates method to study the inelastic transitions in $H^+ + Na$ collisions, Jain and Winter [6] proceeded to perform similar investigations for the $He^{2+} + Na(3s)$ system. Their overall results for state-selective and total electron capture cross sections are in harmony with existing experimental data, but only agree reasonably with previous AOCC calculations performed by Shingal *et al* [7], especially at energy below 10 keV u^{-1} (e.g., see figures 3 and 4 in Jain and Winter [6]). In particular, there exists a noticeable discrepancy between Shingal's 45-state AOCC and Jain and Winter's 74-state SAOCC calculations for the energy dependence of the Na(4p) excitation cross sections. Both sets of results disagree with the available experimental data. It should be noted that both Shingal's and Jain–Winter's AOCC considered some discrete pseudo-continuum states in their calculations.

Recently, Knoop *et al* [8] have utilized the MOTRIMS technique to study single ionization and electron transfer in the $He^{2+} + Na(3s)$ system from 2 keV u^{-1} to 13 keV u^{-1}. They measured state-selective cross sections for capture into the $n = 2, 3, 4$ and $n \geqslant 5$ manifolds and the ionization cross section. The MOTRIMS measured data are compared with classical trajectories Monte Carlo (CTMC) and AOCC calculations. The report showed that the cross sections for capture into $n = 4$ and $n \geqslant 5$ are in good agreement with the CTMC results, while for capture into $n = 2$ and 3, the close-coupling method showed better agreement. As for the single ionization cross sections, both CTMC and 74-state Sturmian atomic-orbital close-coupling (SAOCC74) of Jain and Winter [6] calculations coincide and are in good agreement with the MOTRIMS result at energies above $\sim$8 keV u^{-1}. As the collision energies decrease below 8 keV u^{-1}, the CTMC results demonstrated closer agreement to the experimental measurements, while the SAOCC74 ionization cross sections compared poorly to both experimental measurements and CTMC calculations. The SAOCC74 calculated

ionization cross sections displayed constant energy dependence in the energy range between 2 and 8 keV u^{-1}.

The CTMC calculation shown in Knoop *et al* [8] treats the collision problem within the limit of classical mechanics. The validity of CTMC methods in determining inelastic cross sections in energy regions around the matching velocity (2–13 keV u^{-1}), where quantum mechanics is important, is open to question. Since the semiclassical impact-parameter two-centre atomic-orbital close-coupling (TCAOCC) method has been used extensively with great success in the past in describing the electron capture process in low- and intermediate-energy ion–atom collisions, the motivation behind this work is to employ the same theory but with a large number of pseudostates to investigate the reported discrepancies between close-coupling theory and experimental measurement for the energy dependence of ionization, total, partial and state-selective electron capture and excitation cross sections below 20 keV u^{-1} in He^{2+} + Na(3s) collisions.

This paper is organized as follows. In section 2, the theoretical calculations and choice of basis sets are described. The comparison between the present theoretical results and other theoretical as well as experimental data is given in section 3. Section 4 gives a summary and some concluding remarks.

2. Theoretical model and basis sets

Semiclassical close-coupling (CC) theory of atomic collisions with travelling atomic orbitals (AO) basis expansion method is well known; we refer the reader to [9–11] for details. To determine the inelastic cross sections, we used the same form of theory as in [12, 13]. Briefly, we employed the semiclassical impact-parameter formulation of the close-coupling method with straight-line trajectories for interatomic motion. The time-dependent wavefunction is expanded in terms of bound atomic orbitals plus some discrete pseudo-continuum states (PS) on individual collision partners, each with an appropriate plane wave electronic translational factor. The atomic orbitals are expressed in terms of even-tempered basis functions

$$\phi_{nlm} = \sum_k C_{nk} N_l(\xi_k)\, \mathrm{e}^{-\xi_k r} \tilde{Y}_{lm}(r), \tag{1}$$

where $\tilde{Y}_{lm}(r)$ consists of a spherical harmonic multiplied by r^l; $N_l(\xi_k)$ is a normalization constant and the orbital exponents ξ_k are taken to form a geometric sequence

$$\xi_k = \alpha\beta^k \qquad (k = 1, 2, \ldots, N). \tag{2}$$

The two parameters α and β can be determined by energy minimization. For a low-energy He^{2+} + Na(3s) collision, only the outer electron is active in the inelastic process. The Na atom is treated as a quasi one-electron system with the core frozen. The active electron in the target atom is governed by a model potential:

$$V_{\mathrm{Na}}(r) = -\frac{1}{r}(1 + (10 + 17.9635r)\, \mathrm{e}^{-3.5927r}). \tag{3}$$

The parameters in this model potential are chosen such that the experimental binding energies of the first few states of interest are well reproduced. In fitting the potential parameters the wavefunctions are calculated numerically. Once the potential is chosen, we then make sure that the atomic orbitals are adequately represented by combinations of even-tempered functions, with properly adjusted α and β parameters. The integration of the close-coupled equations with respect to time ($z = vt$) for each impact parameter was carried out from $z_i = -450$ to $z_f = +450$ au. We should point out that, except for the choice of the parameters, the same form of model potential has been used in Jain and Winter [5, 6] and Shingal *et al* [7].

Table 1. Bound and pseudo-continuum states of the He^+ ion up to 83 states in total. The eigenenergies (au) were obtained from diagonalizing the atomic Hamiltonian of the single centre.

n	s	p	d	f	g
1	−2.0000				
2	−0.5000	−0.5000			
3	−0.2222	−0.2222	−0.2222		
4	−0.1250	−0.1250	−0.1250	−0.1250	
5	−0.0800	−0.0800	−0.08000	−0.0800	−0.0800
6	−0.0143	−0.0374	−0.0440	−0.0539	−0.0520
7	0.3364	0.1237	0.0912	0.0064	0.0250
8	1.8996	0.7201	0.7477	0.0289	0.3003
9	12.9445	3.6576			

s: $\alpha = 0.185$; $\beta = 1.342$; $N = 9$.
p: $\alpha = 0.258$; $\beta = 1.224$; $N = 9$.
d: $\alpha = 0.265$; $\beta = 1.255$; $N = 6$.
f: $\alpha = 0.255$; $\beta = 1.265$; $N = 5$.
g: $\alpha = 0.245$; $\beta = 1.453$; $N = 5$.

Table 2. Bound and pseudo-continuum states of atomic Na up to 136 states in total. The eigenenergies (au) were obtained from diagonalizing the atomic Hamiltonian with model potential. The numbers in $(\cdots)$ are experimental data [14].

n	s	p	d	f	g
3	−0.1888 (−0.1889)	−0.1141 (−0.1115)	−0.0556 (−0.0559)		
4	−0.0712 (−0.0716)	−0.0519 (−0.0509)	−0.0313 (−0.0314)	−0.0313	
5	−0.0377 (−0.0376)	−0.0296 (−0.0292)	−0.0198 (−0.0201)	−0.0200	−0.0200
6	−0.0232 (−0.0231)	−0.0188 (−0.0189)	0.0009	−0.0138	−0.0139
7	0.0021 (−0.0157)	−0.0070 (−0.0133)	0.0738	−0.0001	−0.0051
8	0.1255 (−0.0113)	0.0755 (−0.0098)	0.2632	0.0530	0.0289
9	0.5158 (−0.0085)	0.3579	0.7037	0.1978	0.1260
10	1.6211	1.1790	1.6619	0.5581	0.3736
11	4.6863	3.4846	3.6949	1.4264	0.9775
12	13.4233	10.0987	8.2946	3.4970	2.4257

s: $\alpha = 0.087$; $\beta = 1.447$; $N = 15$.
p: $\alpha = 0.067$; $\beta = 1.495$; $N = 13$.
d: $\alpha = 0.115$; $\beta = 1.435$; $N = 12$.
f: $\alpha = 0.086$; $\beta = 1.465$; $N = 11$.
g: $\alpha = 0.096$; $\beta = 1.489$; $N = 11$.

In the present close-coupling calculations with atomic orbitals on the two collision centres, we have a set of 83 atomic states with $l \leqslant 4$ in the He^+ ion. Table 1 shows the energies of the bound and pseudo-continuum states of the He^+ ion. A key element in determining whether the calculated cross sections are stable or not is to see if the results depend on the basis sets used. For this purpose, we generated two different basis sets with $l \leqslant 4$ for the Na target. Due to the limited space available here, table 2 only displays the energies of the bound and pseudo-continuum states of Na target for the basis set 1 which consists of 136 states. For the bound states, the binding energies obtained from the model potential are also compared to experimental values [14]. The basis set 2 is slightly larger (i.e., 145 states) and the energy distribution between these two sets is slightly different (∼5–10%), in particular, for the pseudo-continuum states. The pseudo-continuum states are used in the basis set (i) to help describe the distortion of the electronic orbitals at smaller internuclear separations and (ii) to represent the continua for both projectile and target.

Table 3. Comparison of electron capture cross sections (10^{-16} cm^2) for 219-state and 228-state calculations at collision energies $E = 2$, 5 and 10 keV u^{-1}. The symbols $\bar{s}$, $\bar{p}$, $\bar{d}$, $\bar{f}$ and $\bar{g}$ represent the pseudo-continuum states and the numbers in $[\cdots]$ denote power of 10.

	$E = 2$ keV u^{-1}		$E = 5$ keV u^{-1}		$E = 10$ keV u^{-1}	
σ_{cap}	219-state	228-state	219-state	228-state	219-state	228-state
2s	0.226	0.227	0.225	0.225	0.344	0.345
2p	0.639	0.639	0.594	0.594	1.112	1.107
$n = 2$	0.865	0.866	0.819	0.819	1.456	1.452
3s	9.007	9.010	4.928	4.927	2.082	2.076
3p	31.218	31.218	21.558	21.546	10.857	10.847
3d	75.983	75.983	71.895	71.885	32.985	33.007
$n = 3$	116.208	116.211	98.381	98.358	45.924	45.930
4s	1.835	1.842	1.665	1.667	1.949	1.955
4p	5.866	5.857	6.905	6.887	7.922	7.940
4d	5.797	5.797	14.496	14.489	12.210	12.221
4f	2.888	2.899	10.656	10.655	5.267	5.261
$n = 4$	16.386	16.395	33.722	33.698	27.348	27.377
5s	0.405	0.407	0.660	0.670	1.614	1.570
5p	0.730	0.728	1.606	1.608	4.560	4.520
5d	0.993	0.988	1.307	1.322	4.042	4.035
5f	1.046	1.045	0.683	0.683	1.236	1.237
5g	0.299	0.300	0.900	0.913	0.278	0.284
$n = 5$	3.473	3.468	5.156	5.196	11.730	11.646
$\bar{s}$	3.74[−3]	3.02[−3]	2.84[−2]	1.78[−2]	4.11[−2]	3.79[−2]
$\bar{p}$	1.218[−2]	1.244[−2]	3.405[−2]	4.255[−2]	0.343	0.347
$\bar{d}$	2.00[−2]	2.062[−2]	6.804[−2]	6.947[−2]	0.685	0.680
$\bar{f}$	6.232[−2]	5.538[−2]	0.291	0.292	1.085	1.076
$\bar{g}$	4.172[−2]	4.262[−2]	0.163	0.175	0.767	0.790
Σ_{cap}	0.140	0.134	0.584	0.596	2.921	2.930

Tables 3 and 4 show the stabilities of various cross sections for electron capture and excitation with respect to 219-state and 228-state calculations at three collision energies $E = 2$, 5, 10 keV u^{-1}. We have also generated other basis sets and used them in the calculations but we only present complete results from these two since they have better pseudostate distributions. Both tables indicate that the partial and state-selective cross sections are relatively converged (e.g., $\lesssim$1% for electron capture and an average of ∼10% for excitation) with respect to the number of states used in the present close-coupling calculations. In particular, the inclusion of higher pseudo-continuum states in the target centre has no profound effect on the electron capture (even for capture into the continuum) cross sections. Regarding the excitation process, the discrepancy in the cross sections between the two sets of calculations is also rather small (∼1%) for the dominant channels. A significant difference (∼30%) is only observed for electron transition to pseudo-continuum states at $E = 10$ keV u^{-1}.

3. Results and discussion

We now discuss our final results obtained using the TCAOCC theory described in the previous section. Although Shingal's AOCC results exist, since they disconcertingly agree and disagree with Jain and Winter [6], as well as with the available experimental data, we only considered the Sturmian results from Jain and Winter [6] as a benchmark for comparison. Furthermore,

Table 4. Same as table 3, but for excitation.

	$E = 2$ keV u^{-1}		$E = 5$ keV u^{-1}		$E = 10$ keV u^{-1}	
σ_{ex}	219-state	228-state	219-state	228-state	219-state	228-state
3p	18.629	18.627	24.593	24.605	49.867	49.874
3d	1.820	1.830	1.430	1.448	4.670	4.669
4s	1.166	1.147	0.943	0.946	0.981	0.975
4p	0.614	0.605	0.914	0.914	2.585	2.596
4d	0.216	0.221	0.282	0.282	1.159	1.138
4f	0.340	0.121	0.221	0.071	0.463	0.215
$n = 4$	2.336	2.094	2.360	2.213	5.188	4.924
5s	6.076[−2]	5.967[−2]	0.291	0.294	0.475	0.458
5p	0.192	0.200	0.259	0.262	0.877	0.919
5d	0.161	0.168	0.194	0.239	0.412	0.383
5f	0.223	0.102	0.159	0.104	0.389	0.324
5g	0.146	3.690[−2]	6.224[−2]	7.611[−2]	5.908[−2]	0.542
$n = 5$	1.126	0.914	1.335	1.350	3.352	3.738
$\bar{s}$	1.961[−2]	1.768[−2]	8.253[−2]	4.812[−2]	0.212	0.142
$\bar{p}$	3.759[−2]	4.000[−2]	0.101	8.512[−2]	0.323	0.289
$\bar{d}$	7.573[−2]	5.893[−2]	0.286	0.262	1.323	1.146
$\bar{f}$	5.073[−2]	9.090[−2]	0.141	0.305	0.378	2.181
$\bar{g}$	6.504[−2]	6.303[−2]	0.191	0.172	0.944	0.655
Σ_{ex}	0.249	0.271	0.802	0.872	3.180	4.413

Jain and Winter [6] employed an extended basis set of 74 states while Shingal's AOCC only included up to 45 states. It should also be noted that due to long computing times associated with large numbers of basis functions used in the scattering calculations, throughout this paper we only used the results from the 219-state AOCC calculations instead of those from the 228-state. In addition, tables 3 and 4 have indicated that the calculated electron capture and excitation cross sections are already converged to within ∼2% with the 219-state calculations.

3.1. Single electron capture cross sections

The single electron capture cross sections (in absolute scale) for He^{2+} + Na(3s) as a function of collision energy are shown in figure 1. Theoretical results are given for present AOCC219, SAOCC74 and CTMC, and these three models give somewhat different results. Only the present AOCC219 results, giving larger cross sections below $E = 10$ keV u^{-1}, are in coincidence with the recent experimental data obtained using the MOTRIMS technique [8] for the whole energy range. Nevertheless, the general behaviour of the total capture cross sections as a function of collision energy is well reproduced by both SAOCC74 and CTMC models. In H^+ + Na collisions, Jain and Winter [6] have tested two different types of these model potentials (e.g., see equations (1) and (2) in [6]). Comparing to equation (1), their binding energies for the Na atom obtained using equation (2) agree better with experimental spectroscopic values. They demonstrated that when the correct binding energies of Na(3s) and Na(3p) are enforced in the scattering calculations, their cross sections improved significantly with respect to the experimental data.

Using the model potential (equation (3)), accurate binding energies for Na atom are obtained (see table 2). With the present AOCC219 results agree better with the experimental data, the discrepancies between Jain and Winter's SAOCC74 and the present 219-state

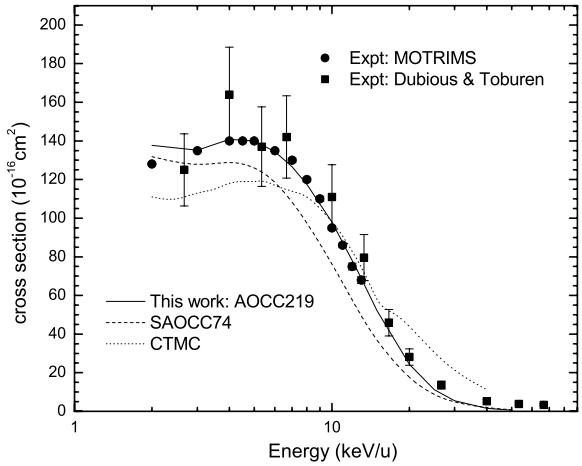

Figure 1. Total electron capture cross sections as a function of collision energy. Comparison of the present AOCC calculations with available theoretical and experimental results. Experimental data: solid circles [8]; solid squares [15].

calculations may be attributed to the inadequacy of the pseudostates representation. Above the 20 keV u^{-1} energy, the previous SAOCC74 results were found to be smaller than the experimental data of Dubious and Toburen [15]. This lead them to believe that the large discrepancy observed between SAOCC74 and experiment may be due to the fact that at such high energies, capture and ionization from inner shells (mostly from L-shell) may play a significant role in the collision dynamics. With the present AOCC219 result practically lying on top of the experimental data of Dubious and Toburen, the conclusion may not be valid.

We now compare the n-resolved partial cross sections with the MOTRIMS experimental data of Knoop *et al* [8], CTMC and SAOCC74 results, as shown in figure 2. At low energy, the electron capture into the $n = 3$ state is the most dominant one, followed by capture into $n = 4$. Both AOCC219 and SAOCC74 are in good agreement with each other; together they are also in better agreement with measurements of Knoop *et al*. The energy dependence of the two curves is well reproduced. The CTMC calculation, however, has underestimated the experimental values by 20% for the capture into $n = 3$, but has reasonably good agreement with AOCC219, SAOCC74 and experimental data for the capture into $n = 4$. Nevertheless, all theories suggest that there is a peak at $\sim$7 keV u^{-1} for capturing into the $n = 4$ state even though the MOTRIMS experiment indicates otherwise—the peak seems to occur at higher collision energy ($\sim$10 keV u^{-1}). Since MOTRIMS techniques could only determine the sum of the partial cross sections for capture into higher n-shells, the associated capture cross sections for all $n > 4$ shells are shown in the last panel. The present AOCC219 calculations (only $n = 5$ and 6 manifolds are considered) are in good agreement with both CTMC and MOTRIMS data, while the cross sections obtained with SAOCC74 are almost one order of magnitude smaller than the present results. Furthermore, AOCC219 has reproduced the shape and together with CTMC has confirmed the experimentally measured sharp maximum at $E = 10$ keV u^{-1}. Again, it is obvious that the discrepancy between the two AOCC calculations is due to the fact that the SAOCC74 basis set only included up to the He^+(4f) state. The missing higher channels are necessary in order to determine these cross sections accurately. Since Jain and Winter did not calculate the $n > 4$ electron capture cross sections, it is important to note that the SAOCC74 $n > 4$ electron capture cross sections depicted here were obtained by

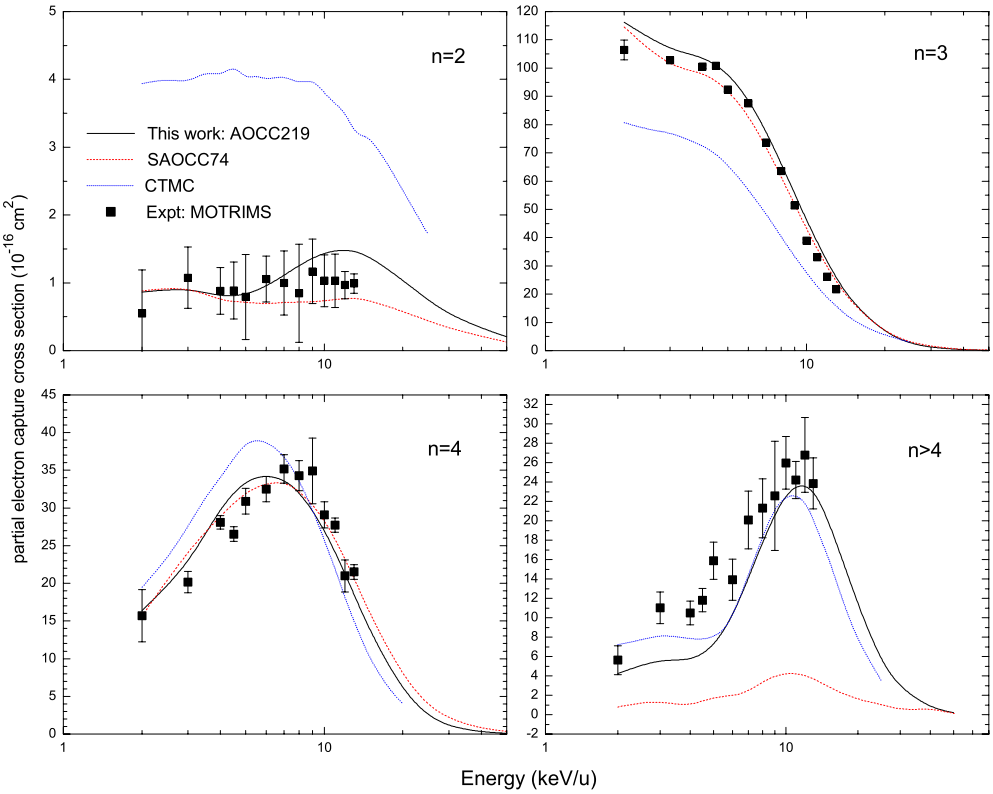

Figure 2. Partial single electron capture cross sections as a function of collision energy. Experimental data: solid squares [8].

subtracting the lower n-shells from the total capture cross sections. Returning to the least dominant channel, the $n = 2$ capture cross sections indicate constant energy dependence. The CTMC calculation has overestimated the cross sections by a factor of 3, while both AOCC methods are in harmony with the MOTRIMS data.

In order to see the relative distribution of various l-orbital subshells within an n-manifold, in figure 3, we present a comparison between the present AOCC219 and SAOCC74 calculations for the state-selective capture cross sections to various $He^+(nl)$ states in the energy range between 2 and 50 keV u^{-1}. Experimental data shown in figure 3(c) are taken from figure 3 of Schippers *et al* [17] and the data are available from 2 to 15 keV u^{-1}. It is clear from these plots that even though the present AOCC219 seems to be consistently slightly higher than the SAOCC74 results for all nl capture channels, both AOCC theories are in good agreement for the range of energies shown here. The AOCC219 also confirmed the previous prediction of SAOCC74 that d-subshells (3d and 4d) are predominant over the rest of the subshells. In addition, our AOCC219 results for capture into He^+(4f) state are in good accord with the experimental data. The cross sections for electron capture into various nl-states along with the collision energies are listed in table 5.

3.2. Single electron excitation cross sections

Figures 4(a) and (b) show our cross sections for the excitation of Na(3p) and Na(3d), respectively. It is obvious that the Na(3p) excitation is the most dominant one in He^{2+} + Na(3s)

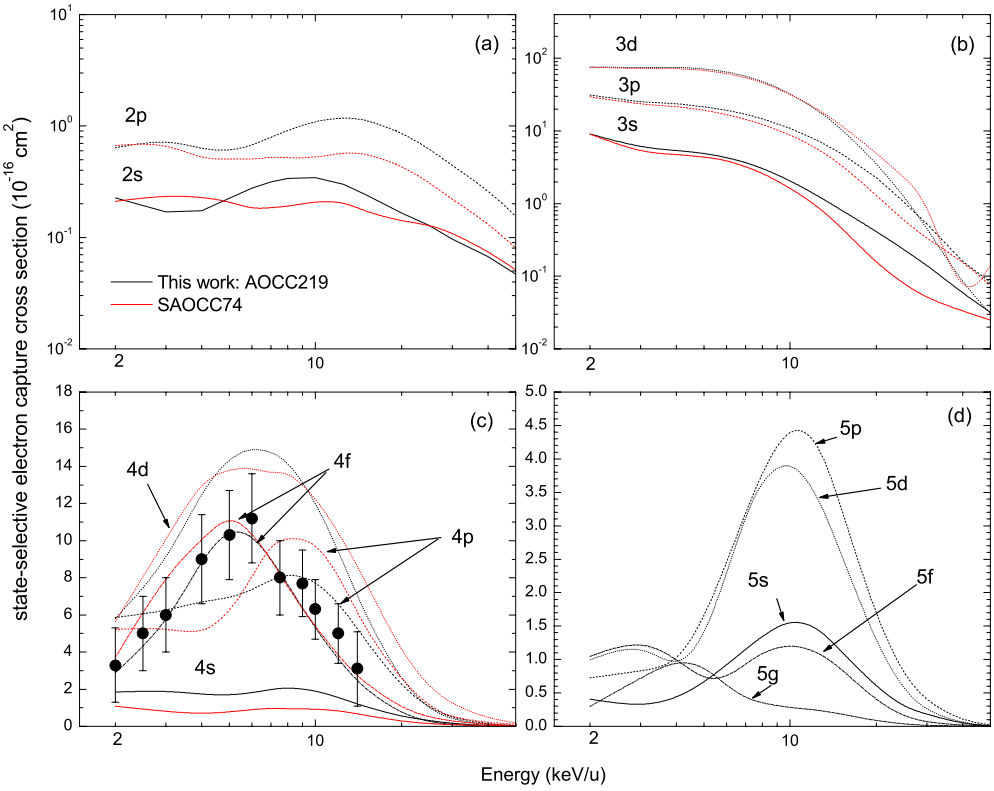

Figure 3. State-selective single electron capture cross sections as a function of collision energy. Theories have colour coding: SAOCC74 (red); AOCC219 (black), Experimental data for electron capture into Na(4f): solid circles [17].

Table 5. Present 219-state electron capture cross sections (10^{-16} cm^2) for He^{2+} + Na(3s) collisions. The numbers in [· · ·] denote power of 10.

keV u^{-1}	2s	2p	3s	3p	3d	4s	4p	4d	4f	5s	5p	5d	5f	5g	Total
2.0	0.23	0.64	9.01	31.20	75.97	1.84	5.87	5.80	2.89	0.41	0.73	0.99	1.05	0.30	137.66
3.0	0.17	0.76	5.85	25.20	75.12	1.92	6.20	8.78	5.43	0.29	0.83	1.27	1.31	0.73	135.23
4.0	0.17	0.62	5.39	23.60	75.37	1.72	6.75	12.70	9.03	0.42	0.92	0.82	1.01	1.00	140.84
5.0	0.23	0.59	4.93	21.60	71.90	1.67	6.90	14.50	10.70	0.66	1.61	1.31	0.68	0.90	139.92
6.0	0.28	0.67	4.33	19.30	65.31	1.81	7.35	15.00	10.30	0.92	2.45	2.29	0.73	0.61	134.48
7.0	0.32	0.79	3.67	16.90	57.06	1.99	7.90	14.80	9.04	1.15	3.19	3.15	0.93	0.43	126.54
8.0	0.34	0.92	3.06	14.70	48.46	2.09	8.24	14.30	7.65	1.35	3.81	3.71	1.11	0.35	117.56
10.0	0.34	1.11	2.08	10.90	32.99	1.95	7.92	12.20	5.27	1.61	4.56	4.04	1.24	0.28	98.02
12.5	0.30	1.20	1.28	7.35	19.33	1.46	6.35	8.83	3.25	1.49	4.32	3.47	1.12	0.25	73.51
15.0	0.24	1.15	0.83	4.95	11.09	1.04	4.58	5.91	1.95	1.13	3.30	2.60	0.87	0.19	52.05
20.0	0.17	0.87	0.41	2.27	3.65	0.52	2.12	2.38	0.67	0.59	1.61	1.23	0.38	0.08	24.30
25.0	0.13	0.62	0.23	1.05	1.26	0.30	0.98	0.91	0.23	0.28	0.77	0.53	0.15	4.0[−2]	11.20
30.0	9.7[−2]	0.44	0.14	0.52	0.46	0.14	0.43	0.35	8.3[−2]	0.18	0.36	0.22	5.8[−2]	1.4[−2]	5.43
40.0	6.7[−2]	0.27	5.8[−2]	0.16	7.8[−2]	0.05	0.13	6.5[−2]	1.7[−2]	3.5[−2]	8.3[−2]	4.5[−2]	1.6[−2]	7.0[−3]	1.59
50.0	4.7[−2]	0.16	3.2[−2]	8.3[−2]	3.1[−2]	1.8[−2]	4.2[−2]	1.8[−2]	1.1[−2]	1.3[−2]	2.2[−2]	9.0[−3]	4.0[−3]	4.0[−3]	0.65

collisions in the presented energy range. The results are also compared with SAOCC74 and experimental data of Schalatmann *et al* [16]. Remarkable agreement is observed in the overall energy dependence of the Na(3p) excitation cross section among the present AOCC, Sturmian

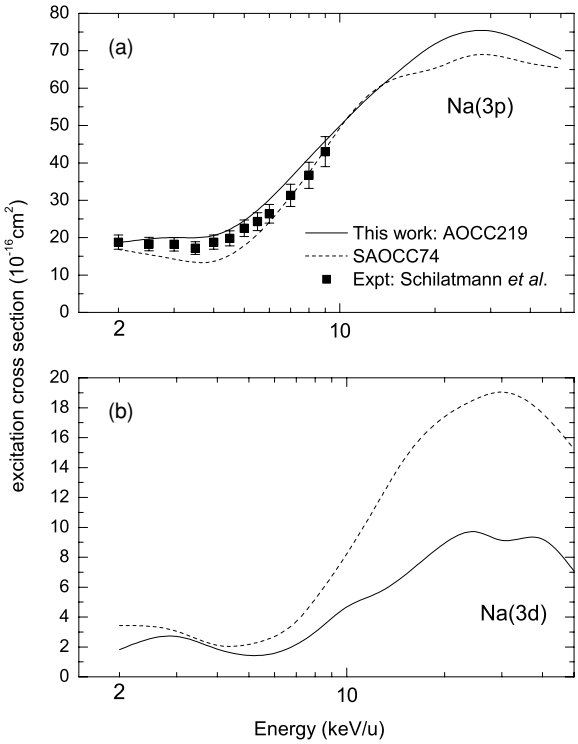

Figure 4. Target excitation cross sections as a function of collision energy. Experimental data: solid squares [16].

and experimental results. It is important to note that both the theoretical results shown here are without cascading effects and it is not clear whether the experimental measurement has included such contributions. As reported in Jain and Winter [6], the cascading effects are expected to be around 12–20% in this energy region.

Since there are no experimental cross sections available for excitation to the Na(3d) state, we can only compare our results with the Sturmian method. We observe a general agreement on the behaviour of the cross sections between the two sets of calculations utilizing different choice and size of the basis sets in the close-coupling approximations, though SAOCC74 results are consistently higher than ours throughout the whole energy range. At $E = 30$ keV u^{-1}, SAOCC74 is a factor of 2 larger than AOCC219. It is worth commenting that Shingal's AOCC results (not shown here) display similar energy dependence but the Na(3d) cross section at 30 keV u^{-1} is about 35% larger than SAOCC74 and 2.5 times larger than the present AOCC219. Evidently, such discrepancy is also due to the limited number of basis sets used in the close-coupling calculations.

We looked further into the 4*l*-subshells excitation and we found similar problems. Figure 5 shows the state-selective Na(4*l*) excitation cross sections. The Sturmian results are consistently larger than the present AOCC219, except for the weakest channel Na(4s) where AOCC219 and SAOCC74 calculated cross sections are comparable. The large discrepancy between the two AOCC calculations may be due to the fact that the SAOCC74 results may have inherented some higher 5*l* and 6*l* excitation components. We believe that with a larger basis set used for SAOCC74, it is possible to resolve the Na(4p) excitation cross section discrepancy between

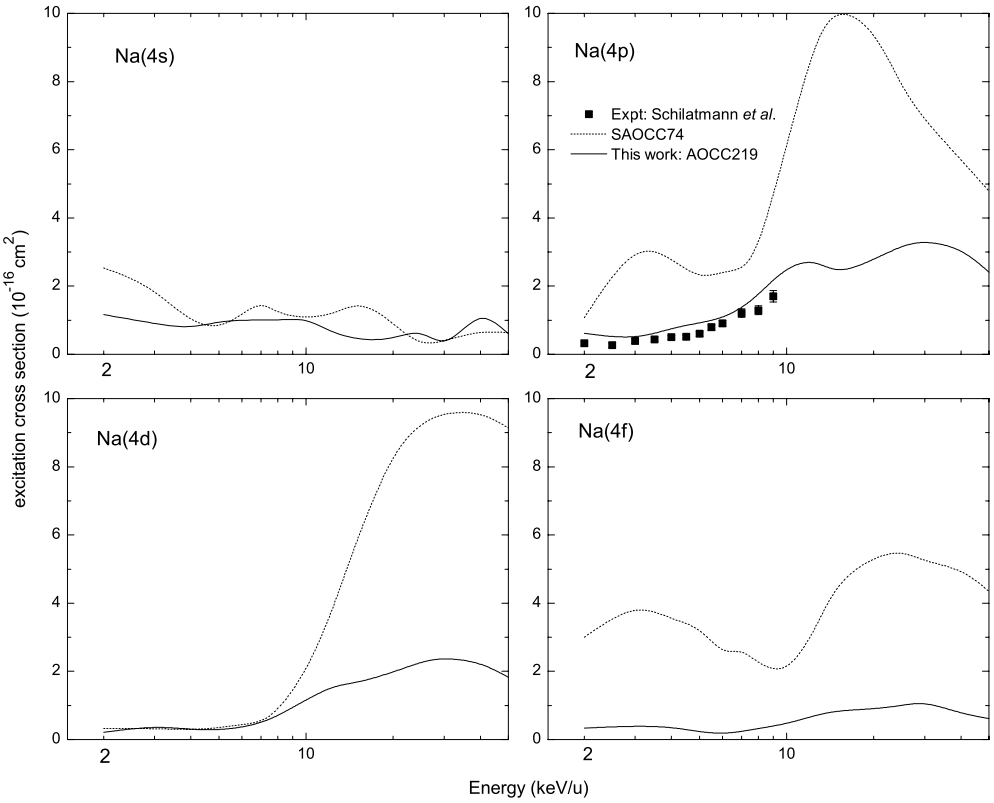

Figure 5. Same as in figure 4, but for Na(4s), Na(4p), Na(4d) and Na(4f) subshells of $n = 4$ manifold of the Na atom. Experimental data: [16].

the SAOCC74 and experimental measurements [16]. Even though our Na(4p) excitation cross sections are slightly higher than the experimental data, both the theory and experiment demonstrate a consistent energy dependence. Table 6 gives a list of the cross sections for target excitation into various *nl*-states together with the collision energies.

3.3. Ionization cross sections

The ionization cross section as a function of collision energy, computed by summing over all the partial cross sections for pseudo-continuum states, is shown in figure 6. Two basis sets (i.e., AOCC219 and AOCC228) are shown together with the SAOCC74, CTMC and MOTRIMS data. The ionization cross section has a sharp increase of roughly two orders of magnitude from 2 to the matching velocity at 13 keV u^{-1}. There are two sets of data from AOCC219—the first set AOCC219T considers the contribution of the pseudo-continuum states from the target centre only while the second one AOCC219TP accounts for the contribution of the pseudo-continuum states from both target and projectile centres.

Although the AOCC219T agrees well with MOTRIMS measurements at 2 and 3 keV u^{-1}, it is clear from the figure that above 3 keV u^{-1} the AOCC219T has significantly underestimated the experimental values by a factor of 2–5. From AOCC219TP, we find the ionization cross sections improved remarkably with respect to the MOTRIMS data if the pseudo-

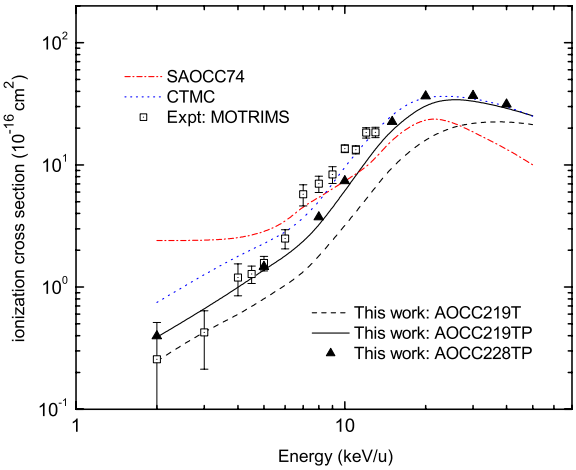

Figure 6. Ionization cross sections as a function of collision energy. Comparison of the present AOCC calculations with available theoretical and experimental results. Present AOCC: AOCC219T—pseudo-continuum states contribution from target centre only; AOCC219TP—pseudo-continuum states contribution from both target and projectile centres; AOCC228TP—same as in AOCC219TP, but with larger basis set size. Experimental data: squares [8].

Table 6. Same as table 5, but for Na(nl) excitation cross sections (10^{-16} cm^2).

keV u^{-1}	Na(3p)	Na(3d)	Na(4s)	Na(4p)	Na(4d)	Na(4f)	Na(5s)	Na(5p)	Na(5d)	Na(5f)	Na(5g)	Total
2.0	18.6	1.82	1.17	0.614	0.216	0.34	6.1[−2]	0.19	0.16	0.22	0.15	23.54
3.0	20.00	2.70	0.91	0.43	0.40	0.40	0.13	0.36	0.19	0.31	0.16	25.98
4.0	20.60	1.85	0.82	0.77	0.29	0.37	0.23	0.26	0.23	0.20	0.09	25.71
5.0	24.60	1.43	0.94	0.91	0.28	0.22	0.29	0.26	0.19	0.16	6.2[−2]	29.36
6.0	30.20	1.58	1.00	1.06	0.36	0.17	0.34	0.31	0.19	0.16	5.2[−2]	35.42
7.0	36.00	2.16	1.01	1.36	0.49	0.24	0.38	0.39	0.19	0.18	5.4[−2]	42.45
8.0	41.30	3.00	1.01	1.75	0.70	0.32	0.41	0.52	0.21	0.25	0.06	49.53
10.0	49.90	4.67	0.98	2.58	1.16	0.46	0.48	0.88	0.41	0.39	0.06	61.97
12.5	58.00	5.63	0.65	2.80	1.59	0.70	0.60	1.16	0.54	0.33	6.8[−2]	72.06
15.0	63.80	6.76	0.47	2.33	1.66	0.85	0.43	0.92	0.52	0.38	0.10	78.21
20.0	71.80	8.94	0.49	2.78	1.97	0.90	9.3[−2]	0.67	1.08	0.63	0.12	89.47
25.0	75.00	9.69	0.59	3.19	2.29	1.00	6.1[−2]	0.73	1.20	0.45	7.7[−2]	94.27
30.0	75.30	9.12	0.40	3.34	2.41	1.12	7.3[−2]	0.83	1.17	0.43	8.9[−2]	94.28
40.0	71.60	9.21	1.05	3.12	2.27	0.77	6.8[−2]	0.76	1.27	0.43	9.1[−2]	90.64
50.0	67.8	7.06	0.61	2.41	1.83	0.62	7.2[−2]	0.67	1.02	0.31	5.5[−2]	82.45

continuum states contribution from both target and projectile centres is considered. To ensure convergence, a larger basis set AOCC228 is also shown in the figure for comparison. Below 6 keV u^{-1}, the AOCC228 and AOCC219 calculated ionization cross sections are practically lying on top of each other. Above 10 keV u^{-1}, the results are probably converged to within ∼20% accuracy and those for AOCC228 are in good accord with CTMC. Overall, the theoretical results presented are in good agreement with the MOTRIMS experiment, except that SAOCC74 demonstrated a constant energy dependence at lower energies.

Finally, in figure 7 we show the ratios of single ionization to single capture as a function of collision energy. An interesting feature of the present results is that the ratios increase with

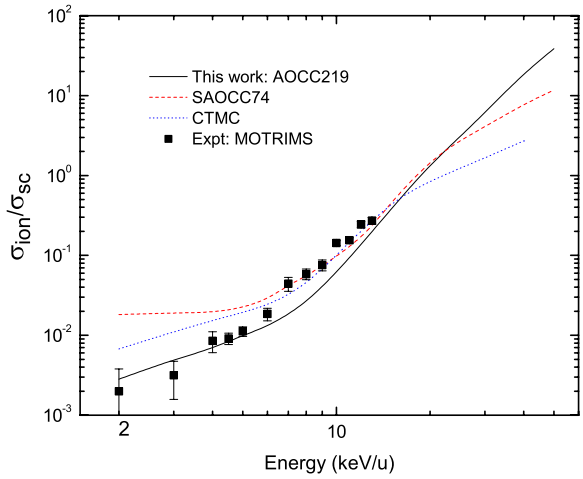

Figure 7. Ratios of single ionization to single capture cross sections as a function of collision energy. Experimental data: solid squares [8].

respect to the collision energy. Below 7 keV u^{-1}, AOCC219 shows better agreement with MOTRIMS data while SAOCC74 and CTMC are much more in accord with experimental data above 7 keV u^{-1}. It is obvious that the ratio is small in the lower energy range as the electron capture process is the most dominant. For instance, at $E = 2$ keV u^{-1} the total electron capture cross section is about 100 times larger than the ionization. As the collision energy increases to matching velocity where the ratio is 1, the ionization and electron capture processes are strongly competing with each other. As the energy increases further, the ionization process takes over and remains dominant while electron capture cross sections decrease precipitously as a function of collision energy. The energy dependence of the ratios $\frac{\sigma_{\rm ion}}{\sigma_{\rm sc}}$ therefore increases as shown in the plot.

4. Summary

In summary, we have performed a detailed close-coupling calculation to investigate the single electron transfer, excitation and ionization cross sections for He^{2+} + Na(3s) collisions from 2 keV u^{-1} to 20 keV u^{-1}. Results from two different basis sets are shown to support the accuracy of the various inelastic cross sections presented. Present cross sections for ionization (total, partial and state-selective), single electron capture and target excitation have been compared with other theories and experimental data in the 2 keV u^{-1} to 20 keV u^{-1} range. With the inclusion of the large number of pseudo-continuum states, the present AOCC method is found to be quite successful in treating the single electron transfer, excitation and ionization process in the present energy range. In particular, the single ionization, total and partial electron capture into $n = 2, 3, 4$ and $n \geqslant 5$ cross sections are in excellent agreement with the recent experimental measurement performed using the MOTRIMS apparatus. Furthermore, the present calculation has resolved the discrepancies observed between 74-state Sturmian AOCC and available experiments. While good agreement between Sturmian AOCC theory and experiment is achieved for predominant transition channels below $E = 20$ keV u^{-1}, we are convinced that the discrepancy between the Sturmian method and experiment for less dominant channels is likely due to the limited number of basis functions used in the scattering

calculation. Finally, we also demonstrated that the contribution of the pseudo-continuum states from the projectile centre is equally important in obtaining an accurate cross section for the ionization process.

Acknowledgments

Support for this work is provided by grant from Office of Basic Energy Sciences (Office of Science, US Department of Energy) administered by Oak Ridge National Laboratory, which is managed by UT-Battelle, LLC under contract no DE-AC05-00OR22725. The author gratefully acknowledges Dr Steven Knoop for providing the MOTRIMS and CTMC data for comparison and Professor Joe Macek and Dr David R Schultz for reading the manuscript.

References

[1] Dowek D, Houver J C, Pommier J, Richter C and Royer T 1990 *Phys. Rev. Lett.* **64** 1713
[2] Houver J C, Dowek D and Richter C 1992 *Phys. Rev. Lett.* **68** 162
[3] Richter C, Anderson N, Brenot J C, Dowek D, Houver J C, Salgado J and Thomsen J W 1993 *J. Phys. B: At. Mol. Opt. Phys.* **26** 723
[4] Roller-Lutz Z, Wang Y, Finck K and Lutz H O 1993 *J. Phys. B: At. Mol. Opt. Phys.* **26** 2697
[5] Jain A and Winter T G 1995 *Phys. Rev.* A **51** 2963
[6] Jain A and Winter T G 1996 *J. Phys. B: At. Mol. Opt. Phys.* **29** 4675
[7] Shingal R, Noble C J and Bransden B H 1987 *J. Phys. B: At. Mol. Phys.* **20** 793
[8] Knoop S, Olson R E, Ott H, Hasan V G, Morgenstern R and Hoekstra R 2005 *J. Phys. B: At. Mol. Opt. Phys.* **38** 1987
[9] Fritsch W and Lin C D 1991 *Phys. Rep.* **202** 1
[10] McDowell M R C and Coleman J P 1970 *An Introduction to the Theory of Ion–Atom Collisions* (Amsterdam: North-Holland)
[11] Bransden B H and McDowell M R C 1992 *Charge Exchange and Theory of Ion–Atom Collisions (The International Series on Monographs on Physics* vol 82*)* (Oxford: Clarendon)
[12] Kuang J Y and Lin C D 1996 *J. Phys. B: At. Mol. Opt. Phys.* **29** 5443
[13] Lee T G, Nguyen H, Flechard X, DePaola B D and Lin C D 2002 *Phys. Rev.* A **66** 042701
[14] http://physics.nist.gov/cgi-bin/AtData/levels_form
[15] Dubious R D and Toburen L H 1985 *Phys. Rev.* A **31** 3603
[16] Schlatmann A R, Hoekstra R, Folkerts H O and Morgenstern R 1992 *J. Phys. B: At. Mol. Opt. Phys.* **25** 3155
[17] Schippers S, Boduch P, van Buchen J, Bliek F W, Hoekstra R, Morgenstern R and Olson R E 1995 *J. Phys. B: At. Mol. Opt. Phys.* **28** 3271